

Thermalization universality-class transition induced by Anderson localization

Weihua Zhang ^{1,2,*} Gabriel M. Lando ^{1,†} Barbara Dietz ^{1,3,‡} and Sergej Flach ^{1,3,§}

¹Center for Theoretical Physics of Complex Systems, Institute for Basic Science, Daejeon 34126, Republic of Korea

²Lanzhou Center for Theoretical Physics and the Gansu Provincial Key Laboratory of Theoretical Physics, Lanzhou University, Lanzhou, Gansu 730000, China

³Basic Science Program, Korea University of Science and Technology, Daejeon 34113, Republic of Korea



(Received 30 August 2023; revised 30 November 2023; accepted 10 March 2024; published 25 March 2024)

We study the disorder-induced crossover between the two recently discovered thermalization slowing-down universality classes, characterized by long- and short-range coupling, in classical unitary-circuit maps close to integrability. We compute Lyapunov spectra, which display qualitatively distinct features depending on whether the proximity to the integrable limit is short or long range. For sufficiently small nonlinearity, translationally invariant systems fall into the long-range class. Adding disorder to such a system triggers a transition to the short-range class, implying a breaking of this invariance, and in the very limit of vanishing nonlinearity Anderson localization emerges. The crossover from the long- to the short-range class is attained by tuning the localization length ξ from $\xi \approx N$ to $\xi \ll N$, where N is the system size. As a consequence, the Lyapunov spectrum becomes exponentially suppressed, depending on the extent to which its translational invariance is destroyed. We expect that this disorder-induced crossover will lead to prethermalized phases and, following quantization, to many-body localization.

DOI: [10.1103/PhysRevResearch.6.L012064](https://doi.org/10.1103/PhysRevResearch.6.L012064)

Thermalization is a universal property of nonintegrable many-body systems, with characteristic timescales that diverge upon approaching integrability [1–7]. In the near-integrable regime, one can interpret the system as a perturbation of an integrable one, with the perturbation’s overall effect being to couple the action-angle variables of the unperturbed system in a nonlinear manner [4–7]. Thermalization slowing-down was shown to strongly depend on the perturbation’s coupling range [5,7,8], which can be classified according to two universality classes: short-range network (SRN) and long-range network (LRN) [5,9–12]. To quantify these slowing-down processes, one can study finite-time averages of observables. These however need to be selected with care [5,11,13] to ensure that one obtains proper ergodization timescales [9–12]. The ambiguity in the choice of suitable observables led to the use of a novel method based on the Lyapunov spectrum (LS) to distinguish the two universality classes [11]. In this approach, which can also be employed to diagnose phase transitions [14–17], significantly more information than the typical Lyapunov time (given by the inverse of the largest Lyapunov exponent) is available, since each

Lyapunov exponent (LE) in the spectrum carries its own characteristic timescale.

The numerical challenges of dealing with weakly nonintegrable many-body Hamiltonian systems led to the study of one-dimensional unitary-circuit maps, for which time evolution is exact. This removes time discretization errors and allows for substantially larger evolution times, and thus for higher resolution in the LS [11,13]. The resulting universal scaling properties of the LS rendered possible an unambiguous identification of the different SRN and LRN universality classes. These were also observed in a recent study of multi-dimensional Josephson-junction networks across all possible lattice dimensions [18]. The predictive power of unitary-circuit maps was thereby confirmed, and above all the LS has been established as an invaluable tool in the study of the thermalization of many-body systems [13].

Our objective is to gain insight into the interplay of disorder with nonintegrability, which might reveal a connection with the celebrated phenomenon of many-body localization [19]. For this, we employ unitary-circuit maps to investigate how the disorder impacts the two thermalization slowing-down universality classes. We use tailored disorder, which leads to Anderson-localized states [20] in the integrable limit of linear maps. The tunable localization length ξ is universal for all eigenmodes and is determined solely by the hoppinglike parameter associated with the unitary-circuit map [21]. We then demonstrate that the system’s thermalization universality class changes from the LRN to the SRN as the localization length is tuned from $\xi \approx N$ to $\xi \ll N$, where N is the system size. Our findings intertwine the fields of many-body localization and thermalization of weakly nonintegrable systems and provide an alternative venue for connecting

* zhangwh2018@gmail.com

† gmlando@ibs.re.kr

‡ bdietzp@gmail.com

§ sergejflach@googlemail.com

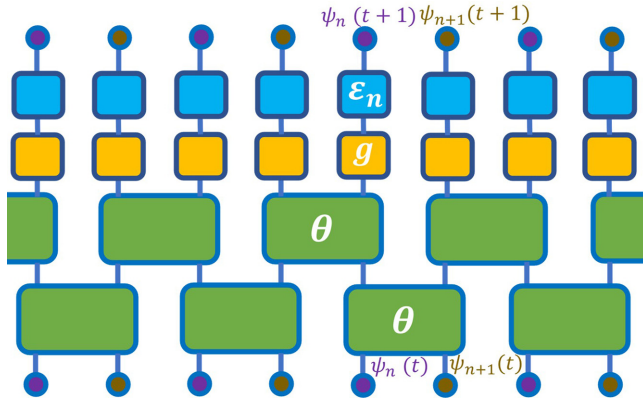


FIG. 1. Schematic representation of the disordered unitary-circuit map, where violet and brown circles indicate sites. Large green blocks represent unitary matrices $\hat{C}(\theta)$, small yellow blocks indicate local nonlinear unitary operators $\hat{G}(g)$, and small blue blocks indicate local disorder unitary operators $\hat{D}(\{\epsilon_n\})$. One time step contains four steps (unitary transformations).

the slowing down of classical many-body dynamics in the presence of disorder and localization physics in quantum many-body systems like the ones proposed in Refs. [22–27].

We employ a modification of the classical unitary-circuit maps introduced in [11,13]. These consist of a one-dimensional periodic chain of N complex numbers ψ_n , with $n = 1, 2, \dots, N$ denoting the sites (we assume that N is even). An initial vector $\vec{\Psi}$ with these complex scalar components ψ_n is evolved by applying iteratively the unitary map

$$\hat{U} = \hat{D}\hat{G}\hat{C}^{(\text{even})}\hat{C}^{(\text{odd})}. \quad (1)$$

Here we interpret the number of iterations as a discrete time, i.e., $\vec{\Psi}(t+1) = \hat{U}\vec{\Psi}(t)$. A pictorial description of \hat{U} is provided in Fig. 1. The operators $\hat{C}^{(\text{even})}$ and $\hat{C}^{(\text{odd})}$ are linear transformations. In matrix representation they are block diagonal with each block consisting of a 2×2 unitary matrix $\hat{C}_{n,n+1}$ with n even and odd, respectively, coupling the components $\psi_n(t)$ and $\psi_{n+1}(t)$, parametrized by a hoppinglike angle parameter θ ,

$$\hat{C}_{n,n+1} \begin{pmatrix} \psi_n(t) \\ \psi_{n+1}(t) \end{pmatrix} = \begin{pmatrix} \cos \theta & \sin \theta \\ -\sin \theta & \cos \theta \end{pmatrix} \begin{pmatrix} \psi_n(t) \\ \psi_{n+1}(t) \end{pmatrix}. \quad (2)$$

All remaining matrix elements are zero and, due to periodicity, $\psi_{N+1} = \psi_1$. Successive applications of $\hat{C}^{(\text{odd})}$ and $\hat{C}^{(\text{even})}$ intertwine neighbors to the left and to the right of site n (green boxes in Fig. 1). In matrix representation the operator \hat{G} corresponds to a diagonal matrix whose elements $\hat{G}_{n,n}$ are nonlinear on-site potentials acting as

$$\hat{G}_{n,n}\psi_n(t) = e^{ig|\psi_n|^2}\psi_n(t). \quad (3)$$

Similar to an anharmonic oscillator whose frequency depends on its level of excitation, the imposed phase shift (during one given time step) depends on the amplitude $|\psi_n|$. This term is responsible for the chaoticity of the dynamics (yellow boxes). Finally, \hat{D} acts on a given site, that is, in matrix representation again is a diagonal matrix with elements

$$\hat{D}_{n,n}\psi_n(t) = e^{i\epsilon_n}\psi_n(t), \quad (4)$$

where the ϵ_n are site-dependent disorder potentials that are uniformly distributed in $[-\pi, \pi]$ (blue boxes). This is a commonly used procedure to introduce on-site disorder. As demonstrated in the following, this is sufficient to induce a transition from the LRN to the SRN.

The unitarity of \hat{U} implies that the total squared norm $|\vec{\Psi}(t)|^2$ is a conserved quantity. Accordingly, in order to allow all possible typical scenarios for the temporal behavior with equal probability, we generated in all considered cases ensembles of trajectories by choosing the initial values of the squared moduli of the rescaled components $\eta_n = N|\psi_n|^2$ uniformly spread over the N sphere with the joint-probability distribution $P(\{\eta_n\}) \propto \delta(N - \sum_{n=1}^N \eta_n)$. This yields, for the probability distribution of the η_n , $P(\eta) \propto (1 - 1/N)(1 - \eta/N)^{N-2} \xrightarrow{N \gg 1} e^{-\eta}$. For the computation of the LS Λ comprising the LEs Λ_i with $\Lambda_1 \geq \Lambda_2 \geq \dots \geq \Lambda_N$, we follow the calculation procedure of Ref. [13], outlined in more detail in [28]. Note that we are considering the part of the LS that is composed of non-negative LEs in the spectrum. We can do so because, similarly to time-independent Hamiltonian systems, the N positive LEs come in pairs with negative ones of the same modulus $\Lambda_i = -\Lambda_{2N-i+1}$ [13]. The final simulation time is denoted by T_s .

In the absence of hopping, achieved by setting $\theta = 0$, the sites decouple and the squared norms $|\psi_n|^2$ are conserved. This results in N functionally independent conserved quantities. Since the system has N degrees of freedom implying a $2N$ -dimensional phase space, this limit is integrable. The squared norms then provide a discrete analog to the actions in continuous Hamiltonian systems when $\theta = 0$ [11,13]. A second integrable limit is realized by setting $g = 0$. In this case, the sites remain coupled, but there is no source of nonlinearity, and the squared norms of the corresponding normal modes, i.e., of the eigenvectors of $\hat{U}(g = 0)$, are conserved [11,13].

Let us consider first the disorder-free case. When approaching the decoupled integrable limit, i.e., when $\theta \ll 1$, each action is only weakly coupled to its nearest neighbors, resulting in a SRN [11,13]. In the regime $g \ll 1$, on the other hand, all normal-mode actions are weakly coupled to each other such that all-to-all linear interactions persist and implicate a LRN [11,13]. Furthermore, it was demonstrated that, in the absence of disorder, the Lyapunov spectra for LRN and SRN systems behave significantly differently as the integrable limit is approached: While most of the LEs in the LRN class are of the same order of magnitude at any distance from the integrable limit, the LEs in the SRN class are damped and end up spanning several orders of magnitude, with the span increasing upon approaching the integrable limit (see Fig. 2). We derived an ansatz for the rescaled Lyapunov spectrum $\bar{\Lambda}$ of the LRN and SRN. This rescaled spectrum is obtained by dividing the original LEs by the maximal LE (MLE) $\bar{\Lambda}_i = \Lambda_i/\Lambda_1$. The starting point of the derivation is the analytical result for the number of Lyapunov exponents $N(\Lambda)$ below $\Lambda = \Lambda_i$, given by $N(\Lambda_i) = N + 1 - i$, $i = 1, 2, \dots, N$. Away from the limiting values $0 < \bar{\Lambda}_i < 1$, this number is well described by the integrated Wigner semicircle law [29–31], yielding an inverse semicircle law for $\bar{\Lambda}$ versus $\rho_i = i/N$. The damping rate of the spectrum in the SRN regime, on the other hand, is exponential. An approximation of the resulting

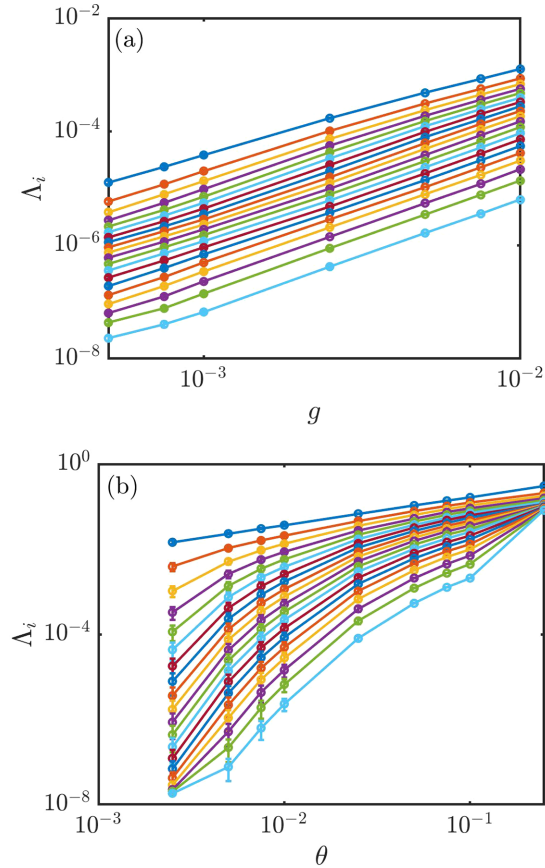


FIG. 2. Lyapunov spectra Λ_i of the ordered unitary-circuit map versus (a) g in the LRN regime ($\theta = 1.13$ and $T_s = 10^8$) and (b) θ in the SRN regime ($g = 1$ and $T_s = 10^9$). The error bars show the standard deviation σ_g obtained from an ensemble of 12 different trajectories. Here $N = 200$.

expression, which for $\rho > 0$ reflects these features, is provided by the ansatz

$$\overline{\Lambda(\rho)} = (1 - \rho^\alpha) e^{-\beta \rho^\gamma}. \quad (5)$$

The parameters α , β , and γ are determined from the fit of this ansatz to the rescaled LS. However, the qualitative behavior of $\overline{\Lambda(\rho)}$ is already well captured with $\gamma = 1$ [18]. We confirmed the applicability of the ansatz for various parameter settings and illustrate it in Fig. S4 of [28] for one ordered case and the corresponding disordered case. In addition, we compute the rescaled Kolmogorov-Sinai (KS) entropy $\kappa = \frac{1}{N-1} \sum_{i=2}^N \bar{\Lambda}_i = \int_0^1 \bar{\Lambda} d\rho$, which is a very useful quantifier of the different regimes. In the SRN regime, κ tends to 0 when approaching the integrable limit, while in the LRN regime, it saturates at some value, as shown in Fig. 3. The insets of Fig. 3 show that the fitting parameter α does not vary significantly for all considered cases. In contrast, the exponent β grows with a power law in the SRN upon lowering θ , while it saturates similarly to α in the LRN with decreasing g . As a consequence, the rescaled LS $\bar{\Lambda}(\rho)$ saturates on some analytic invariant curve in the LRN for $g \rightarrow 0$, and knowing one LE (e.g., the MLE) results in knowing all others as well, whereas the SRN is characterized by an exponential damping of LEs compared to the MLE.

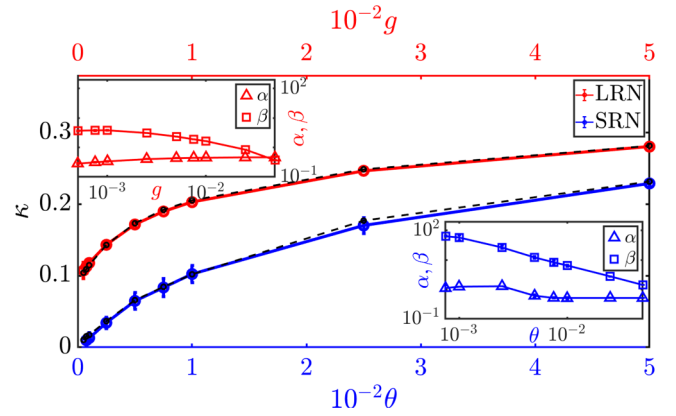


FIG. 3. Rescaled KS entropy κ for the ordered case in the LRN regime with $\theta = 1.13$ (red circles, top) versus g in the SRN regime with $g = 1$ (blue circles, bottom) versus θ . Solid lines connect the data points and guide the eye. Here $T_s = 10^8$ and $N = 200$. The insets show the fit coefficients α (triangles) and β (squares) of Eq. (5) in the LRN (top left) and SRN (bottom right) regimes. The error bars represent the standard deviation deduced from an ensemble of 12 trajectories. The dashed curves in the main plot show the integral of Eq. (5) evaluated with the coefficients from the fits.

Figures 2 and 3 show results for Lyapunov spectra and KS entropy for the ordered case. Our next objective is to compare them to results for the disordered case to get insight into the effect of disorder on the LRN with the aim of realizing a SRN for weak but nonzero nonlinearity $g \ll 1$ and establishing a connection to Anderson localization [20,32,33]. For $g = 0$, all normal-mode eigenstates of \hat{U} are exponentially localized [21]. The localization length ξ depends only on the hopping-like parameter θ ,

$$\frac{2}{\xi} = |\ln(|\sin \theta|)|, \quad \xi(\theta \rightarrow 0) \rightarrow 0, \quad \xi\left(\theta \rightarrow \frac{\pi}{2}\right) \rightarrow \infty. \quad (6)$$

Let us expand an arbitrary $\vec{\Psi}(t)$ in the eigenmode basis at $g = 0$ and $\hat{U}(g=0)\vec{\Psi}_k = e^{i\omega_k} \vec{\Psi}_k$, namely, $\vec{\Psi}(t) = \sum_k c_k(t) \vec{\Psi}_k$. Here the eigenmodes $\vec{\Psi}_k$ are Anderson localized with components $|\psi_k^n| \sim e^{-|n|/\xi}$. The quasienergies ω_k are real and the expansion coefficients $c_k(t)$ are complex. The actions $\{|c_k|^2\}$ are the constants of motion. Away from the integrable limit, i.e., for $0 < g \ll 1$, the expansion coefficients are coupled as

$$c_k(t+1) = e^{i\omega_k} c_k(t) + ig \sum_{k_1, k_2, k_3} e^{i(\omega_{k_1} + \omega_{k_2} - \omega_{k_3})} I_{k, k_1, k_2, k_3} c_{k_1}(t) c_{k_2}(t) c_{k_3}^*(t), \quad (7)$$

where I_{k, k_1, k_2, k_3} is an overlap integral $I_{k, k_1, k_2, k_3} \sim \sum_n \psi_{k_1}^n \psi_{k_2}^n (\psi_{k_3}^n)^* (\psi_k^n)^*$. For small g and $|\frac{\pi}{2} - \theta|$ the length ξ becomes larger than the system size, implying that the normal modes extend over the entire system, and Eq. (7) turns into a LRN with essentially all-to-all action couplings. For small g and $\theta \ll 1$ the length ξ tends to zero, the eigenmodes are strongly localized, and Eq. (7) turns into a SRN with essentially nearest-neighbor action couplings.

We therefore predict that the universality class of a finite disordered system will depend on the ratio ξ/N . In Fig. 4 we

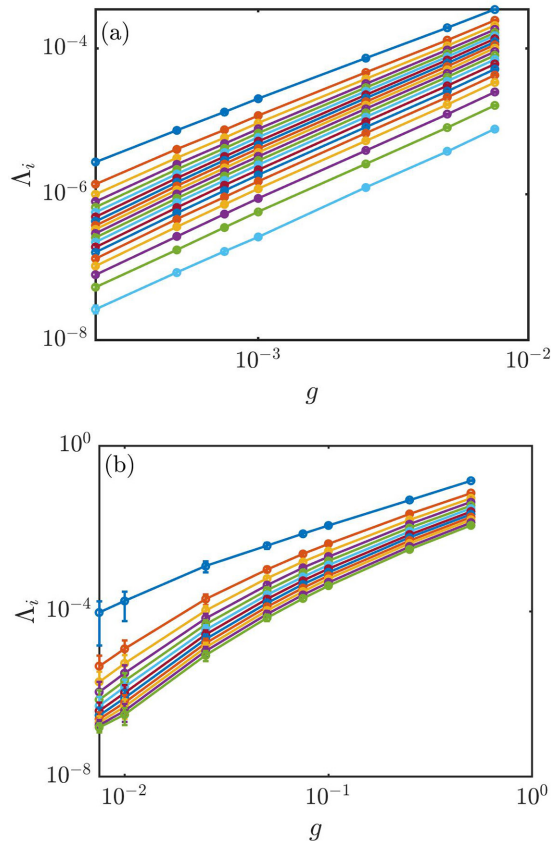


FIG. 4. Lyapunov spectra Λ_i for the disordered case for (a) the LRN with $\theta = 1.26$ and $\xi \approx 40$ and (b) the SRN with $\theta = 0.38$ and $\xi \approx 2$. Here Λ_i is plotted versus g for $T_s = 10^8$ and $N = 200$. The error bars show the standard deviation σ_g for an ensemble of 100 trajectories.

show the LS dependence on g for $\xi/N = 0.2$ [Fig. 4(a)] and $\xi/N = 0.01$ [Fig. 4(b)]. We clearly observe that Fig. 4(a) displays the typical LRN behavior observed in Fig. 2 with all LEs being proportional to each other. In Fig. 4(b) the LEs widen in a fanlike way, indicating SRN features.

To gain further insight, we extrapolate the rescaled LS down to $g = 0$ [28] as a function of θ and fit the ansatz (5) to the outcome. The results are summarized in Fig. 5 and for α in Fig. S5 of Ref. [28]. Figure 5(a) shows the dependence $\xi(\theta)$ for convenience. Figure 5(b) exhibits the dependence of the exponent β on θ (closed squares), i.e., on the localization length ξ with a growth over several decades, as expected, when crossing over from a LRN to a SRN class. In Fig. 5(c) the dependence of the asymptotic rescaled KS entropy κ_a versus θ is plotted (closed circles), showcasing the vanishing of κ_a for small θ . For reference, we plot in Figs. 5(b) and 5(c) the corresponding results for the ordered case using open symbols. In this case no sizable change of $\beta(\theta)$ and $\kappa_a(\theta)$ is observed. In addition to inducing the transition from a LRN to a SRN by varying the localization length ξ , this can be achieved by increasing the system size N . To demonstrate this, we have calculated the quantity κ_a for different system sizes, all with the same localization length $\xi = 2$, exhibited in Fig. S6 of Ref. [28], yielding that κ_a indeed decreases with increasing system size N .

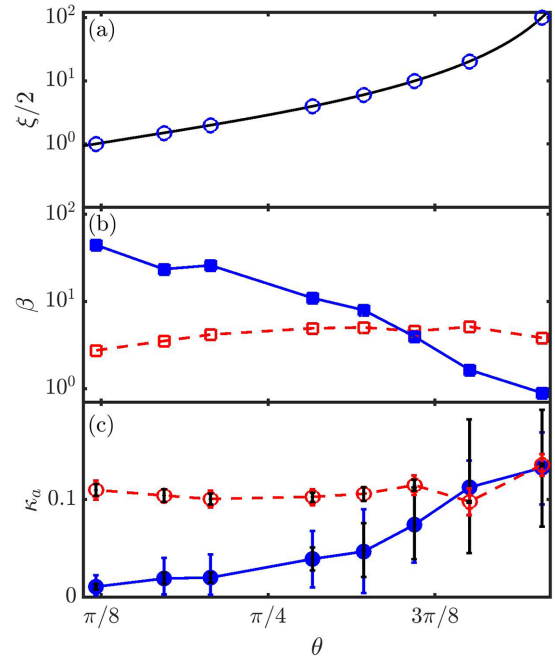


FIG. 5. Disordered case after extrapolating down to $g = 0$. Ordered case results are added for comparison. (a) Localization length ξ versus θ . The black line is the analytical result of Eq. (6) and the blue circles mark the θ values used for the computations. (b) Fit coefficient β of the asymptotic rescaled LS $\bar{\Lambda}(\rho; g \rightarrow 0)$ versus θ (closed blue squares). Open red squares are obtained from the corresponding ordered case data [28]. (c) Asymptotic rescaled KS entropy κ_a versus θ (closed blue circles). Open red circles are obtained from the corresponding ordered case data [28]. The error bars represent the time σ_t (black) and ensemble σ_g (blue and red) standard deviations [28]. Lines guide the eye.

The Lyapunov spectrum (or better the inverse of its Lyapunov exponents) captures the timescale of thermalization. These times diverge in a qualitatively different way upon approaching integrable limits for short- and long-range network classes. Previous studies used the limit of weak lattice coupling to realize a SRN, while weak nonlinearities resulted in a LRN. Here we show that the addition of disorder allows us to realize a SRN in the limit of weak nonlinearities, which in many situations correspond to weak two-body interactions. To achieve our goals we compute the rescaled Lyapunov spectrum and fit the ansatz (5) to it to extract an exponent whose divergence signals the presence of a SRN and measure the rescaled KS entropy of the rescaled LS as another highly useful quantifier to tell SRN and LRN regimes apart. We also extrapolate the rescaled LS down to vanishing nonlinearity strength. These procedures allow us to unambiguously identify the crossover from a long-range network to a short-range network in a disordered system upon reducing the localization length.

Let us discuss and speculate about some consequences of the observed crossover. Approaching the integrable limit in the regime of a short-range network implies that at any time the dynamics of the system is mostly regular, with rare local spots of nonlinear resonances leading to weak chaos (which is probably associated with the largest Lyapunov exponent). The

density of these rare spots diminishes the closer the system is tuned to the integrable limit. Large but finite systems are therefore expected to display prethermalization features, where certain parts of the system show thermal properties which will fluctuate from part to part. Additional quantization of the considered systems might lead to a suppression of chaotic resonances and prethermalization and ultimately to many-body localization related features. It remains to be studied whether the well-defined short-range network regimes of the studied classical systems will indeed result in many-body localization for the corresponding quantum systems, at variance with the long-range network classes.

Our studies were confined to finite system sizes. We expect that the thermodynamic limit $N \rightarrow \infty$ will result in a short-

range network class for all cases of finite localization length (see Sec. VII of Ref. [28]). It remains to be studied whether large but finite values of the localization length will or will not result in qualitative changes of the Lyapunov spectrum scaling in the limit of weak nonlinearities and infinite system size.

This work was supported by the Institute for Basic Science in Korea through Project No. IBS-R024-D1. W.Z. acknowledges financial support from the China Scholarship Council (Grant No. CSC-202106180044). W.Z. also acknowledges financial support from the NSF of China under Grants No. 11775100, No. 12247101, and No. 11961131009. We thank Tilen Čadež and Alexei Andreanov for fruitful discussions.

-
- [1] K. Huang, *Statistical Mechanics*, 2nd ed. (Wiley, New York, 1987).
- [2] G. Bel and E. Barkai, Weak ergodicity breaking in the continuous-time random walk, *Phys. Rev. Lett.* **94**, 240602 (2005).
- [3] M. Rigol, Breakdown of thermalization in finite one-dimensional systems, *Phys. Rev. Lett.* **103**, 100403 (2009).
- [4] C. Danieli, D. K. Campbell, and S. Flach, Intermittent many-body dynamics at equilibrium, *Phys. Rev. E* **95**, 060202(R) (2017).
- [5] C. Danieli, T. Mithun, Y. Kati, D. K. Campbell, and S. Flach, Dynamical glass in weakly nonintegrable Klein-Gordon chains, *Phys. Rev. E* **100**, 032217 (2019).
- [6] T. Mithun, C. Danieli, Y. Kati, and S. Flach, Dynamical glass and ergodization times in classical Josephson junction chains, *Phys. Rev. Lett.* **122**, 054102 (2019).
- [7] T. Mithun, C. Danieli, M. V. Fistul, B. L. Altshuler, and S. Flach, Fragile many-body ergodicity from action diffusion, *Phys. Rev. E* **104**, 014218 (2021).
- [8] A. S. de Wijn, B. Hess, and B. V. Fine, Lyapunov instabilities in lattices of interacting classical spins at infinite temperature, *J. Phys. A: Math. Theor.* **46**, 254012 (2013).
- [9] T. Goldfriend and J. Kurchan, Equilibration of quasi-integrable systems, *Phys. Rev. E* **99**, 022146 (2019).
- [10] S. Ganapa, A. Apte, and A. Dhar, Thermalization of local observables in the α -FPUT chain, *J. Stat. Phys.* **180**, 1010 (2020).
- [11] M. Malishava and S. Flach, Thermalization dynamics of macroscopic weakly nonintegrable maps, *Chaos* **32**, 063113 (2022).
- [12] M. Baldovin, A. Vulpiani, and G. Gradenigo, Statistical mechanics of an integrable system, *J. Stat. Phys.* **183**, 41 (2021).
- [13] M. Malishava and S. Flach, Lyapunov spectrum scaling for classical many-body dynamics close to integrability, *Phys. Rev. Lett.* **128**, 134102 (2022).
- [14] C. Dellago and H. A. Posch, Lyapunov instability, local curvature, and the fluid-solid phase transition in two-dimensional particle systems, *Physica A* **230**, 364 (1996).
- [15] C. Dellago and H. A. Posch, Lyapunov instability in the extended XY-model: Equilibrium and nonequilibrium molecular dynamics simulations, *Physica A* **237**, 95 (1997).
- [16] B. Hadrien and H. A. Posch, What does dynamical systems theory teach us about fluids? *Commun. Theor. Phys.* **62**, 451 (2014).
- [17] A. S. de Wijn, B. Hess, and B. V. Fine, Chaotic properties of spin lattices near second-order phase transitions, *Phys. Rev. E* **92**, 062929 (2015).
- [18] G. M. Lando and S. Flach, Thermalization slowing-down in multidimensional Josephson junction networks, *Phys. Rev. E* **108**, L062301 (2023).
- [19] A. Pal and D. A. Huse, Many-body localization phase transition, *Phys. Rev. B* **82**, 174411 (2010).
- [20] P. W. Anderson, Absence of diffusion in certain random lattices, *Phys. Rev.* **109**, 1492 (1958).
- [21] I. Vakulchyk and S. Flach, Universal anderson localization in one-dimensional unitary maps, *Chaos* **33**, 083134 (2023).
- [22] A. Chan, A. De Luca, and J. T. Chalker, Solution of a minimal model for many-body quantum chaos, *Phys. Rev. X* **8**, 041019 (2018).
- [23] A. Chan, A. De Luca, and J. T. Chalker, Spectral statistics in spatially extended chaotic quantum many-body systems, *Phys. Rev. Lett.* **121**, 060601 (2018).
- [24] Y. Li, X. Chen, and M. P. A. Fisher, Quantum Zeno effect and the many-body entanglement transition, *Phys. Rev. B* **98**, 205136 (2018).
- [25] A. Nahum, S. Vijay, and J. Haah, Operator spreading in random unitary circuits, *Phys. Rev. X* **8**, 021014 (2018).
- [26] B. Skinner, J. Ruhman, and A. Nahum, Measurement-induced phase transitions in the dynamics of entanglement, *Phys. Rev. X* **9**, 031009 (2019).
- [27] Y. Li, X. Chen, and M. P. A. Fisher, Measurement-driven entanglement transition in hybrid quantum circuits, *Phys. Rev. B* **100**, 134306 (2019).
- [28] See Supplemental Material at <http://link.aps.org/supplemental/10.1103/PhysRevResearch.6.L012064> for details on the unitary circuit map, equations of evolution, and some details on Lyapunov spectrum computation.
- [29] M. L. Mehta, *Random Matrices* (Academic, London, 1990).
- [30] G. Gur-Ari, M. Hanada, and S. H. Shenker, Chaos in classical D0-brane mechanics, *J. High Energy Phys.* **02** (2016) 091.
- [31] M. Hanada, H. Shimada, and M. Tezuka, Universality in chaos: Lyapunov spectrum and random matrix theory, *Phys. Rev. E* **97**, 022224 (2018).
- [32] E. Hamza, A. Joye, and G. Stolz, Dynamical localization for unitary Anderson models, *Math. Phys. Anal. Geom.* **12**, 381 (2009).
- [33] A. Lagendijk, B. van Tiggelen, and D. S. Wiersma, Fifty years of Anderson localization, *Phys. Today* **62** (8), 24 (2009).